(Received 7 September 2025, Accepted 11 November 2025, Scheduled 21 November 2025)

A Dual-Band Four-Element MIMO Antenna with Triangular Slots and Hexagonal Rings for GSM, Wi-Fi, LTE, 5G, and IoT Applications

Sachin S. Khade[1,*], Nikhil Mangrulkar[2,*], Chitra Khade[3], Sapana Dhanvijay[4], and Prasanna L. Zade[1]

[1] *Yeshwantrao Chavan College of Engineering, Nagpur, India*
[2] *Symbiosis Institute of Technology Nagpur Campus, Symbiosis International (Deemed University), Pune, India*
[3] *GHRCEM, Nagpur, India*
[4] *PBCOE, Nagpur, India*

ABSTRACT: A novel compact four-element MIMO antenna system is developed, featuring a rectangular microstrip patch structure integrated with dual vertical grooves. The projected antenna design incorporate slits, triangular slot, and DGS to realize dual-band resonance with simultaneously multiband response and mitigating mutual coupling effects. The antenna operates effectively at 0.9 GHz and 2.4–2.6 GHz bands, supporting multiple IoT and wireless communication standards such as GSM (0.9 GHz), Lora (2.4 to 2.5 GHz), Wi-Fi (2.4 GHz), Bluetooth (2.4 GHz), LTE (Band 8, Band 7, Band 41 and Band 53), and 5G (n8, n41). The antenna demonstrates satisfactory impedance matching, achieving return losses of −16.16 dB at 0.94 GHz and −31.19 dB at 2.496 GHz, with isolation levels exceeding −15 dB. The antenna delivers stable far-field radiation with 2.8–3.6 dBi gain, and prototype validation demonstrates strong agreement with simulations, confirming its suitability for compact, high-performance IoT (2.4 GHz) and 5G Sub-6 GHz devices.

1. INTRODUCTION

Multiple-input multiple-output (MIMO) technology has emerged as a cornerstone in modern wireless communication which enables higher data rates, improved reliability, and spectral efficiency. Due to the rapid evolution of 5G, beyond-5G (B5G), and 6G networks, compact multi-element MIMO antennas have become critical for supporting both sub-6 GHz and mmWave frequency ranges [1, 2]. Despite remarkable progress, recent MIMO antenna designs exhibit several constraints. High-frequency mmWave prototypes [1, 2], achieve excellent isolation and very low envelope correlation coefficient (ECC) through defected ground structure (DGS) and decoupling slots but are highly sensitive to fabrication tolerances, restricting large-scale deployment. Among them, four-port MIMO antennas represent an optimal tradeoff between spatial diversity and structural complexity, making them highly suitable for wearable devices, smartphones, vehicular systems, and Internet of Things (IoT) platforms [3–5].

The major challenge in MIMO antenna design is minimizing its mutual coupling while maintaining a compact structure. Multiple techniques such as electromagnetic band gap (EBG) structures and DGS are very effective to suppress surface waves and improving isolation [6, 7, 24]. Ultra-wideband (UWB) solutions [4, 6, 13–15, 20, 21] offer wideband coverage, yet their large footprints and ground modifications limit miniaturization for smartphones and IoT platforms. Mushroom-like EBG units and etched ground-plane slots is very useful to enhance isolation by disrupting surface current distribution [11, 12]. Sub-6 GHz patch and DGS-based antennas [5, 7, 11, 12, 16] provide compactness and improved isolation but only narrow bandwidth and modest gain. Other methods such as stub loading, symmetrical slotting, and L-shaped decoupling elements have reliably brought isolation levels above 15 dB with envelope correlation coefficients (ECC) below 0.05 [13–15]. Flexible and wearable antennas [3, 14, 18] enable compact integration but suffer from detuning, impedance mismatch, and reduced robustness under bending. For mmWave arrays, irregular layouts and ground-plane modifications reduce element interaction and broaden impedance bandwidth [26, 28].

Innovative antenna geometries play a crucial role in achieving wideband operation and compactness. Various designs or shapes are preferred during designing the antenna which include circular and elliptical patches, U-shaped monopoles, folded-meander radiators, asymptote-inspired structures, and fractal slots [11–16]. Fractal and slot-based geometries are very compact and provides multiband response. It also supports band-notch features to suppress WLAN and Wi-MAX interference [18, 19]. Ground-plane optimization techniques have further enabled dual-band and hybrid satellite-terrestrial sub-6 GHz operation [8, 10]. These geometrical innovations confirm diversity performance while keeping the antenna suitable for integration into small devices.

Reconfigurable MIMO antennas are gaining significant traction due to their ability to dynamically adapt frequency bands. Positive-intrinsic-negative (PIN) diodes, radio frequency micro-electro-mechanical system (RF-MEMS) switches, and

* Corresponding authors: Sachin S. Khade (sac_mob@rediffmail.com); Nikhil Mangrulkar (mangrulkar.nikhil@gmail.com).

metasurface integration have been used to enable dual-band and multi-band reconfigurability [10, 20, 25, 27]. Reconfigurable approaches [20, 21] introduce PIN diodes and resonators but suffer from added biasing networks and efficiency loss. Balancing compactness, wideband operation, isolation, and manufacturability remains a central challenge. With the help of switches, the utilization of optimized spectrum and interference suppression is possible in heterogeneous communication environments. In a few cases, the meandered ground lines and stepped resonators have been combined with antenna to achieve twin band LTE and 5G application with better isolation [22, 30], whereas in the UWB designs, antenna produces band-rejection response which is useful for cognitive radio applications.

A recent trend in antenna research is the integration of artificial intelligence (AI) and machine learning (ML) for enhancing antenna geometries and decoupling strategies. Deep learning frameworks and graph neural networks have been employed to tune parameters and predict performance outcomes with greater precision [9, 25, 28, 29]. Metasurface and high-isolation designs [9, 19, 23, 27] enhance performance at the expense of thickness, cost, and fabrication complexity. This approach is mainly relevant for compact mmWave arrays, where manual optimization becomes impossible due to complex electromagnetic interactions. AI-driven optimization facilitates faster design cycles and greater efficiency in attaining targeted performance metrics.

Four-port MIMO antennas are increasingly personalized to meet the requirements of specific application domains. In vehicle-to-everything (V2X) and vehicular systems communication systems, the environment is dynamic; therefore, for better pattern diversity, robust isolation, and reliable communication, a compact quad-port configuration using edge-coupling and slot-loading techniques is suitable [3, 6]. Quad-port design provides a compromise between diversity gain and design simplicity, which make them highly appropriate for smartphones and IoT sensors [4, 9]. For wearable and body-area network (BAN) applications, low-profile, conformal, and flexible designs are required; additionally, they must ensure a low specific absorption rate (SAR) to confirm user safety. These antennas are predominantly well matched for 5G NR FR2 wearable platforms, where compactness, flexibility, and high isolation are crucial [9, 14, 17].

2. METHODOLOGY

A compact four element MIMO antenna was designed using rectangular microstrip patch, with twin vertical grooves. The patch has been designed strategically to form multiple resonances to encompass vertical tracks, thus expanding the impedance band width and allowing multi-functional bands to accommodate different IoT communication standards like Wi-Fi. The geometry was precisely optimized to achieve compactness while maintaining high return loss and acceptable gain across all bands. The methodology consists of following key points.

2.1. Single Element

The proposed antenna makes it well suited for low-power, short-range applications due to its compact size. The main aim of design is to address the need for affordable, high-efficiency antennas which have capability to support the next-generation IoT infrastructure.

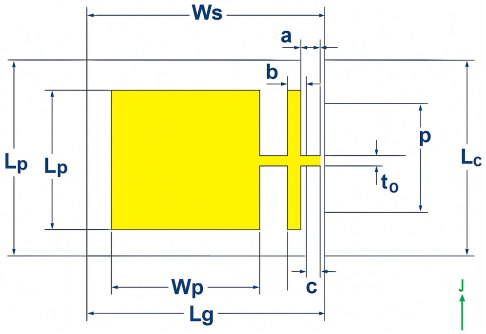

FIGURE 1. Geometry of patch.

The antenna's geometry is illustrated in Figure 1, and a parametric analysis has been done for fine-tuning of the structure to achieve dual-band operation and extended bandwidth. Overall, the slotted microstrip patch antenna offers a compact and high-performance solution for sub-6 GHz 5G, IoT, and Wi-Fi 6E applications. The detailed design parameters for proposed antenna are listed in Table 1.

TABLE 1. Dimensions of the projected antenna.

Parameters	**Ls**	**Ws**	**Lp**	**Wp**	**Lg**	**Wg**
Values (mm)	38	30	26	18	38	59
Parameters	**a**	**b**	**c**	**d**	**e**	**f**
Values (mm)	2	2	2	8.5	3	8.5

2.2. Configuration of MIMO Antenna

The antenna geometry revealed in Figure 2 consists of four patch elements arranged in a square configuration, each with a distinct slot and fin structure. In Figure 2(a), the precise dimensions reveal that each element features a unique patch geometry with slots and triangular cutouts, which are likely used to alter the resonant frequency, control impedance, and improve bandwidth. The four patches are arranged in quad pattern within a size of $60 \times 60\,\text{mm}^2$ to enhance gain and diversity performance. The placement, orientation, and spacing of the patches support controling mutual coupling and reducing interference between elements. The triangular slot shapes inside each patch can introduce perturbations to the surface current distribution. These perturbations can create multiple resonant modes and better impedance bandwidth. Overall, this geometry aims to achieve a compact size MIMO antenna for modern wireless communication systems.

2.3. Evolution of Geometry of MIMO Antenna

The evolution of patch depicted in Figure 3 begins with a basic quad structure using four rectangle-shaped radiating elements which are equipped with slits, slots, and stubs for

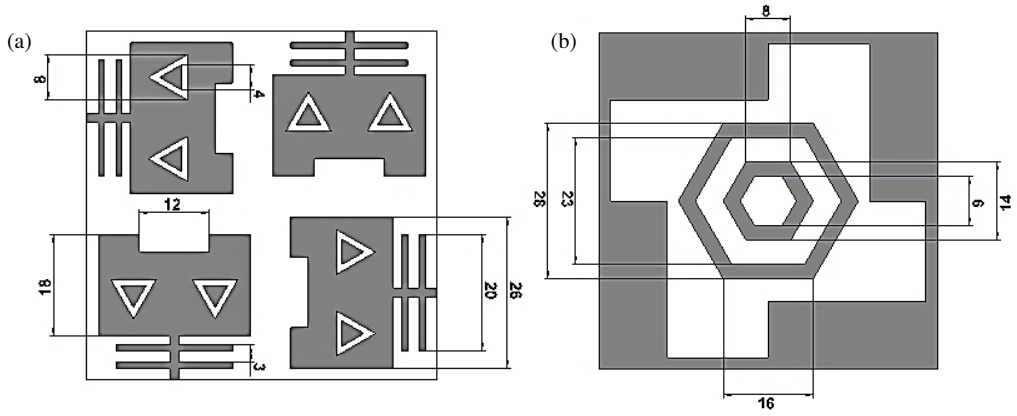

FIGURE 2. Four element MIMO antenna. (a) Front view. (b) Ground plane.

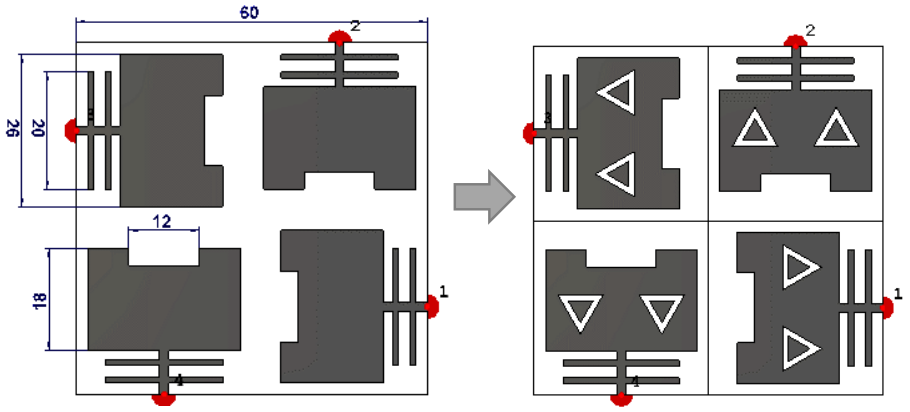

FIGURE 3. Evaluation of patch of MIMO antenna.

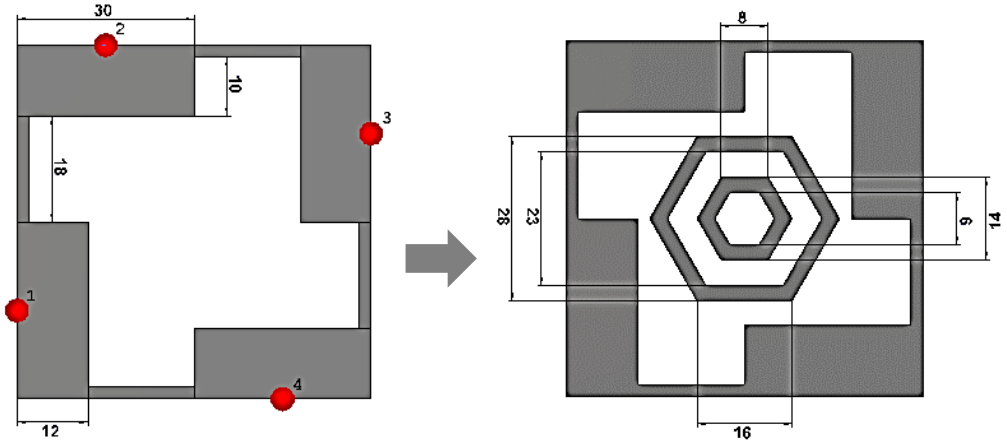

FIGURE 4. Evaluation of ground plane of MIMO antenna.

impedance matching and resonance tuning. In the modified design, triangular slots are introduced inside the rectangular patches to increase the effective surface current and allowing multi-resonance behavior. Hence, the evolution of a simple slit-loaded patch to a optimized slot-etched design effectively enhances frequency performance.

Figure 4 illustrates that the modifications to the ground plane geometry in a MIMO antenna influence its impedance matching, as reflected in S-parameter results. In the first figure, the ground plane is a stepped rectangular structure with feed points at four different positions, designed to control current flow and minimize the coupling between elements. The second figure indicates modified ground plane that integrates twin concentric hexagonal ring, which modifies the current distribution and increases the electrical length of antenna. The introduction of slits, slots, and ring shapes creates additional resonant paths,

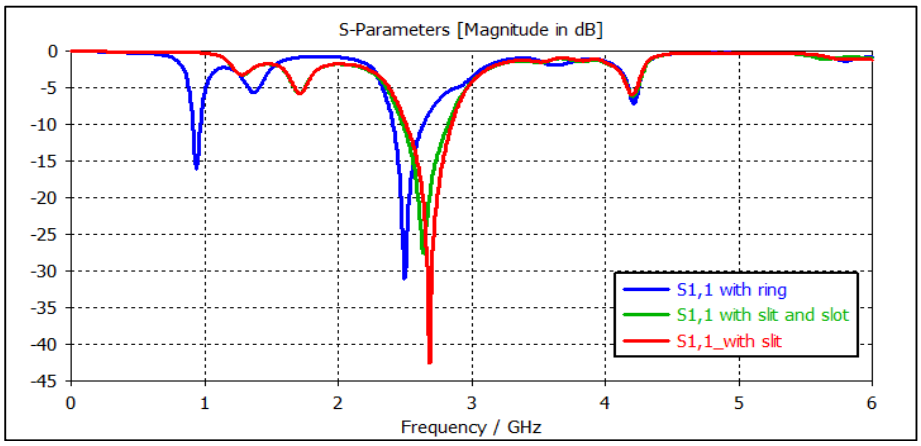

FIGURE 5. Parametric results with modification.

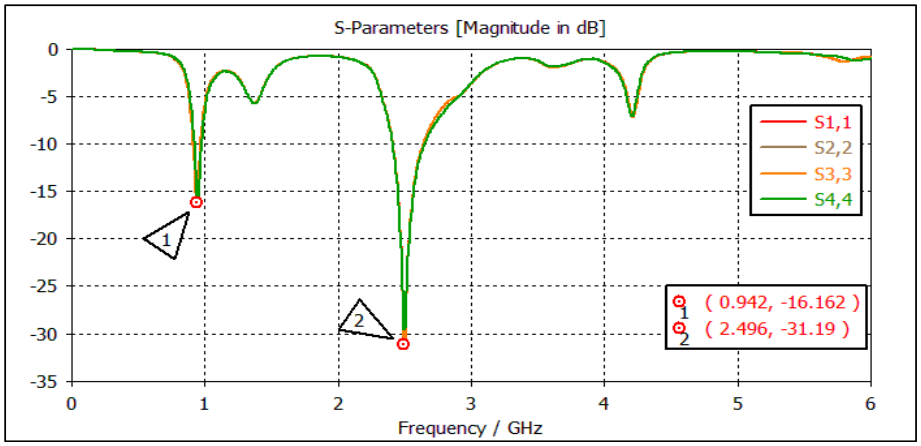

FIGURE 6. Reflection coefficient of final MIMO antenna.

also improves impedance matching at desired frequencies, and suppresses unwanted harmonics.

Figure 5 indicates three configurations. The first "slit only" design (red) produces deep resonance near 2.8 GHz with good matching but less multi-band behavior; the second "slit and slot" design (green) shifts the resonance a little bit and improves the impedance matching over a wider range; the third "ring" design (blue) achieves multiple resonances, enhancing low-frequency response around 0.94 GHz while maintaining reasonable matching with higher frequency at 2.5 GHz. These changes demonstrate how ground plane modification directly impacts the antenna's resonant modes and provides multiple operating bands.

3. RESULT AND DISCUSSION

Figure 6 shows the reflection coefficients for all four ports of a MIMO antenna, which gives identical performance across all the ports, indicating good symmetry in the antenna design. The graph reveals two primary resonant frequencies: the first at approximately 0.94 GHz with a return loss of -16.16 dB and the second at around 2.496 GHz with a deeper return loss of -31.19 dB. A deeper notch indicates stronger impedance matching and less reflection at a higher frequency. For balanced MIMO performance, there should be minimal variation in impedance matching between elements, as demonstrated in Figure 6. As we got better matching, higher gain, and better efficiency at higher frequency bands, the reasonable return loss at the lower frequencies indicates satisfactory performance. Overall, the results confirm that the antenna operates efficiently at two different frequency bands, making it appropriate for dual bands.

Figure 7 presents the transmission coefficient characteristics of MIMO antenna which indicates mutual coupling between four-port MIMO antennas. This is a critical factor for reducing interference and improving MIMO performance. The coupling characteristics between consecutive and opposite elements exhibit slight variations. At the operating frequency of 0.94 GHz, the transmission coefficient between consecutive elements is approximately -17 dB, indicating a relatively low level of mutual coupling. However, at the second resonant band (2.5 GHz), this value is found around -12 dB, suggesting a moderate coupling effect at higher frequencies. Overall, the S-parameter re-

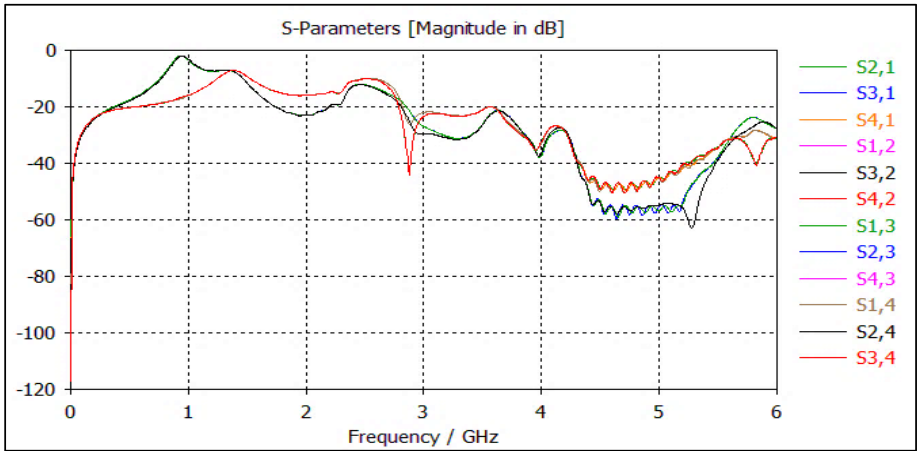

FIGURE 7. Transmission coefficient of final MIMO antenna.

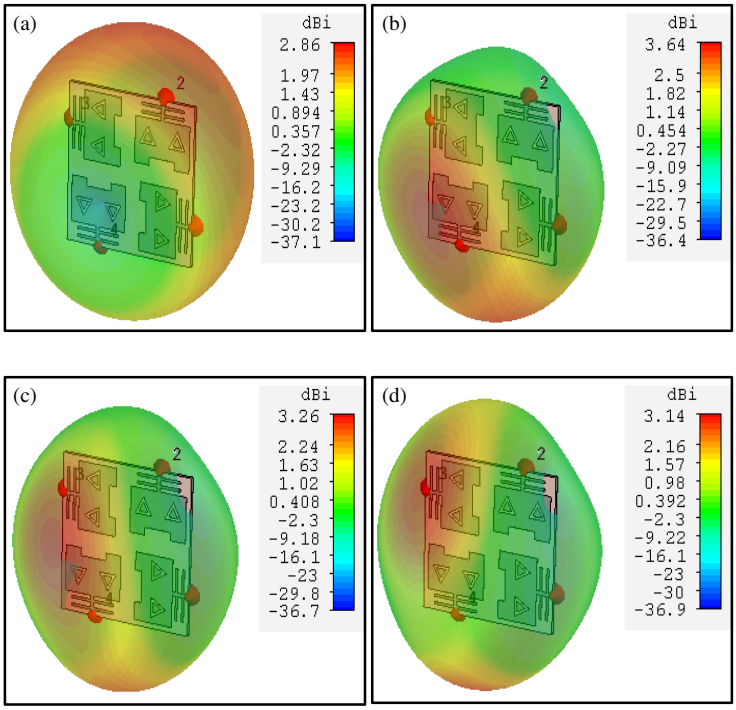

FIGURE 8. 3D radiation pattern of antenna. (a) 0.9 GHz, (b) 2.4 GHz, (c) 2.5 GHz, (d) 2.6 GHz.

sults confirm that the antenna achieved good impedance matching at its operating bands and maintains better port isolation, which is crucial for efficient MIMO communication.

The 3D radiation patterns of the proposed antenna array are simulated at several frequencies. Figure 8 displays the 3D radiation patterns at 0.9, 2.4, 2.5, and 2.6 GHz frequencies. The antenna exhibits a gain of 2.86 dBi at 0.9 GHz band. The antenna reveals a significant improvement in radiation efficiency at higher frequencies. The greater efficiency and comfortable gain make this frequency band suitable for applications such as Wi-Fi and Bluetooth. The performance of antenna remains consistent around 2.5 GHz, and it achieves good efficiency and stable radiation characteristics. This indicates that the antenna is properly matched and optimized for the extended 2.4 to 2.5 GHz ISM band. The antenna continues to provide stable efficiency at 2.6 GHz range. The nearly uniform gain across the 2.4–2.6 GHz band highlights its suitability for LTE and WLAN applications. From the results, it can be observed that the antenna operates in a dual-band configuration, covering both sub-GHz (0.9 GHz) and 2.4–2.6 GHz ISM/LTE bands. The higher frequency bands (2.4–2.6 GHz) give much better performance with gain values ranging from 3.1 to 3.6 dBi. This makes the antenna capable for IoT and wireless communication devices, where dual-band operation is essential for global system for mobile communications or long range radio (GSM/LoRa) (sub-GHz) as well as Wi-Fi/Bluetooth/LTE (2.4–2.6 GHz).

The proposed antenna's 2D radiation characteristics, evaluated in the E-plane ($\theta = 90°$), highlight the frequency-

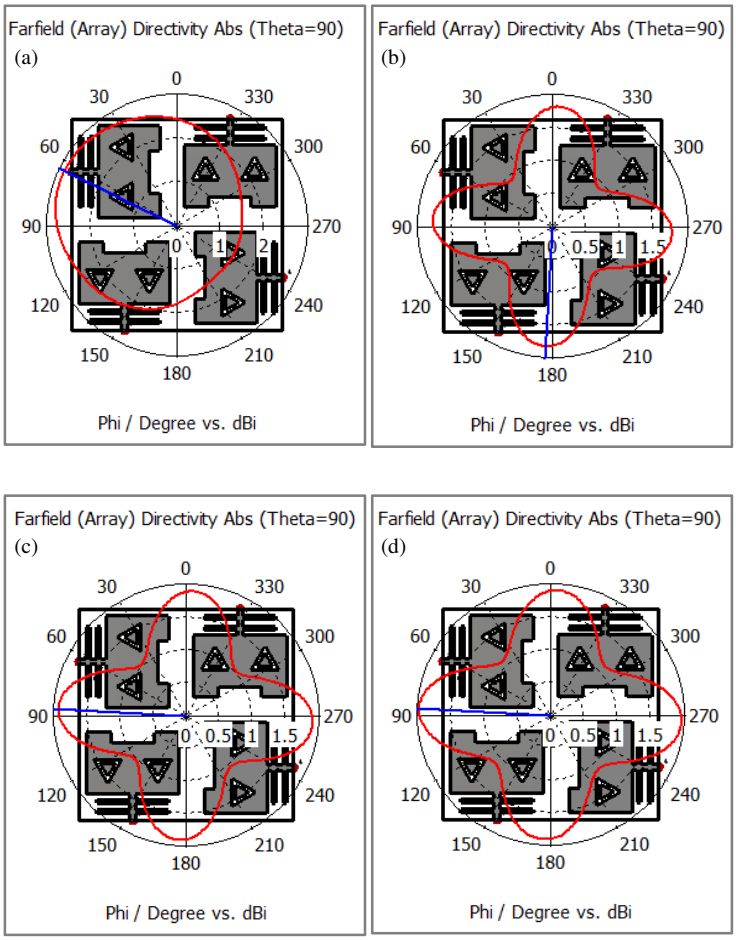

FIGURE 9. 2D E plane (co-polarization) radiation pattern of antenna. (a) 0.9 GHz, (b) 2.4 GHz, (c) 2.5 GHz, (d) 2.6 GHz.

dependent variations in main lobe angle and amplitude. As presented in Figure 9, the antenna exhibits a main lobe magnitude of 2.9 dBi with a tilted radiation direction at 64° at 0.9 GHz, indicating some asymmetry due to structural effects at sub-GHz operation. In contrast, at frequency 2.4 GHz, the main lobe magnitude falls to 1.8 dBi and produce more symmetric bidirectional radiation. The main lobe magnitude is slightly improved to 1.91 dBi and 1.96 dBi with increases in frequency to 2.5 GHz and 2.6 GHz, respectively, indicating more stable and consistent radiation behavior in the ISM band.

Figure 10 indicates the current distribution of proposed antenna at 0.9, 2.4, and 2.4 GHz. At 0.9 GHz, the antenna primarily carries current alongside its edges, which signifies the fundamental resonant mode. The triangular slots extend the path of the current, allowing the antenna to resonate effectively at this lower frequency. When the frequency increases to 2.4 GHz, the current becomes stronger and more concentrated around the triangular slots and patch edges. This indicates a higher-order mode, which improves radiation efficiency and makes the antenna suitable for wireless uses like WLAN and Bluetooth. At 2.5 GHz, the current remains highly focused near the slots and radiating edges, confirming another resonant mode close to 2.4 GHz. The hexagonal ring patch also plays a critical role by influencing the ground plane currents. These return currents mirror the patch's shape and intensify around edges, corners, and discontinuities as frequency rises. At resonance, dense loops are formed on the ground plane, enhancing impedance matching, bandwidth, and overall radiation performance.

The performance of the proposed antenna can be assessed through envelope correlation coefficient (ECC) and diversity gain (DG) plots. The ECC shown in Figure 11 indicates the correlation between different antenna elements. The ECC should remain below 0.5 for efficient MIMO operation, to ensure good diversity and low correlation between antennas. The results indicate that the ECC values for antenna pairs (1 & 2 and 1 & 3) are well below this threshold value across the operating band and thus enhance system capacity and reliability.

Figure 12 indicates the diversity gain. Ideally, the value of diversity gain should be close to 10 dB, and the plotted results achieve values near this optimum across most of the frequency range. These results collectively confirm that the antenna gives low signal correlation and strong diversity performance, which make it effective for reliable, high-capacity MIMO communication.

Figure 13 shows group delay versus frequency for four port combinations. Group delay indicates signal distortion across frequencies. Most traces remain near zero, but sharp dips occur around 1.5, 2.5, and 4.5 GHz, especially for paths 1-to-1

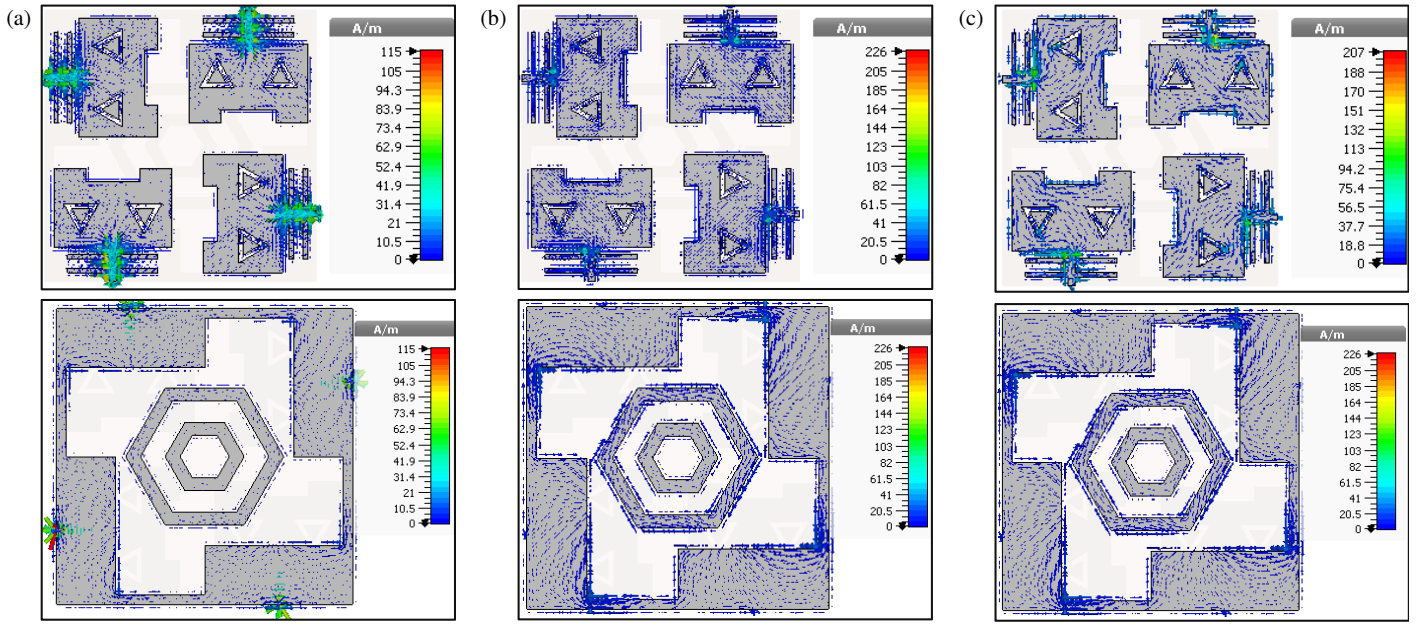

FIGURE 10. Current distribution of antenna. (a) 0.9 GHz, (b) 2.4 GHz, (c) 2.5 GHz.

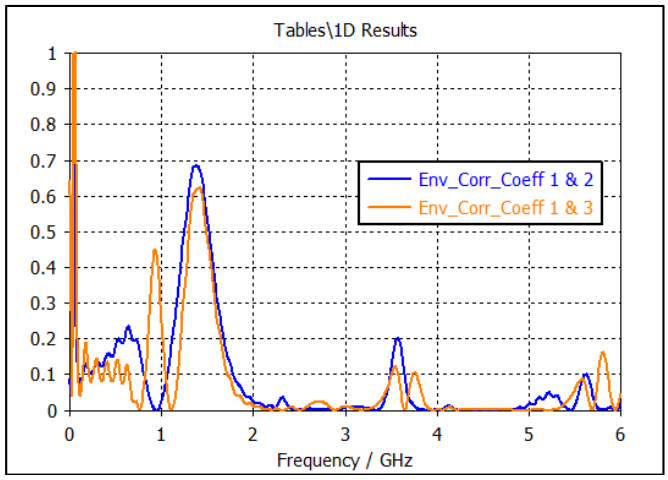

FIGURE 11. ECC between consecutive and cross element.

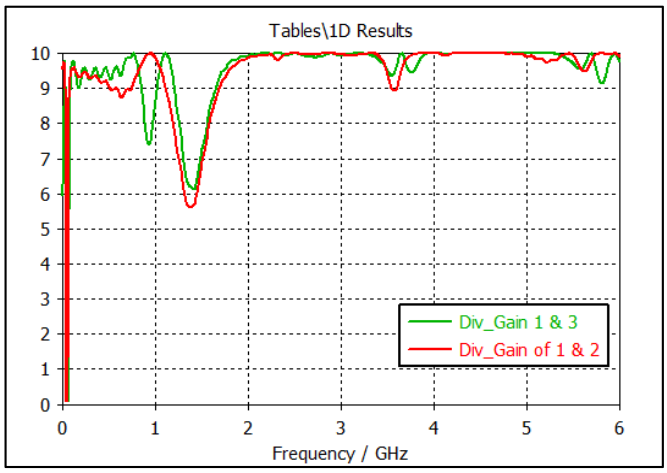

FIGURE 12. Diversity gain between consecutive and cross element.

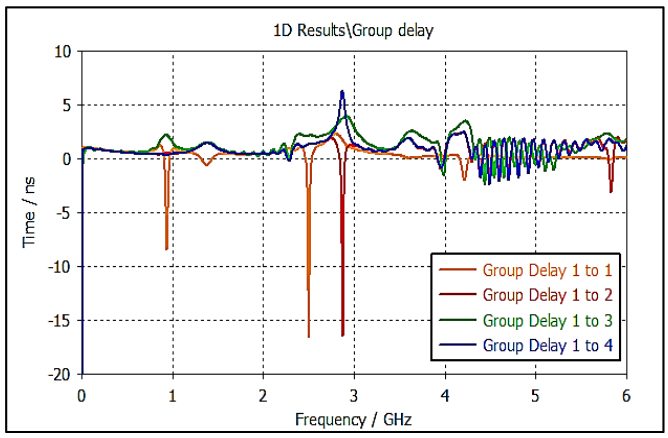

FIGURE 13. Group between consecutive and cross antenna elements.

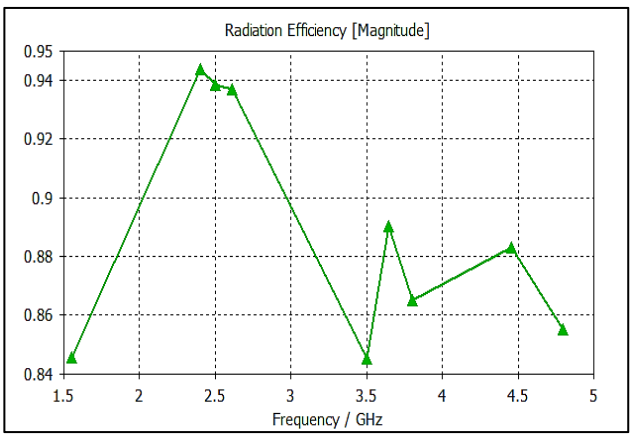

FIGURE 14. Radiation efficiency of antenna.

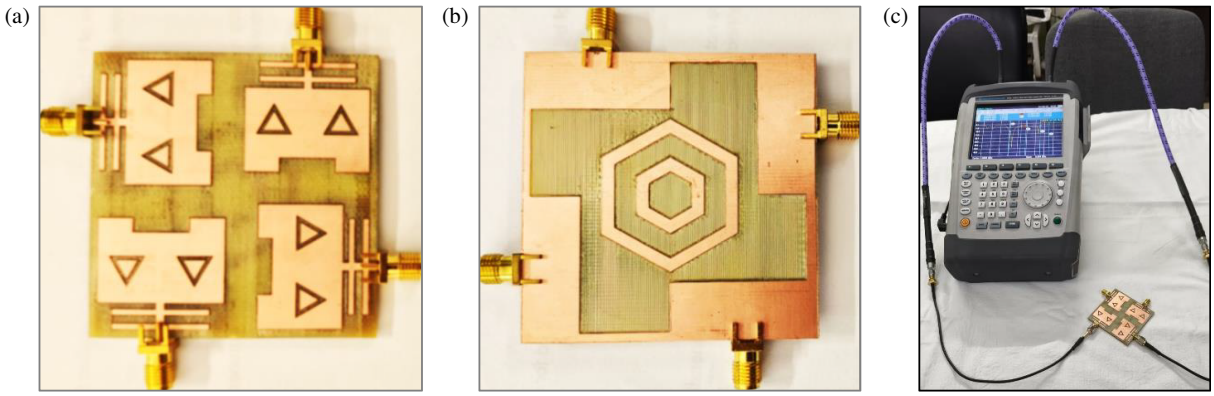

FIGURE 15. Fabricated prototype of four element MIMO antenna. (a) Front view. (b) Ground plane. (c) Measuring setup.

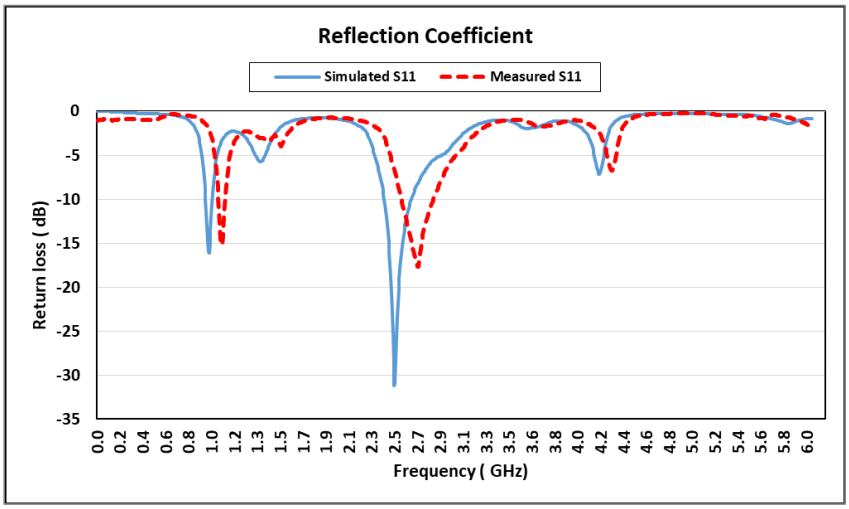

FIGURE 16. Simulated vs measured reflection coefficient of MIMO antenna.

and 1-to-2, suggesting distortion. The 1-to-4 path shows high-frequency oscillations above 4 GHz, indicating potential resonance or reflections affecting signal integrity in that range. Figure 14 indicates the radiation efficiency of an antenna. It gives the conversion of input power into radiated energy and ranges from approximately 0.84 to 0.95. The efficiency peaks around 2.4 to 2.5 GHz, reaching a maximum about 94.5 %, indicating excellent performance in that band — ideal for applications like Wi-Fi or Bluetooth.

4. FABRICATED PROTOTYPE

Figure 15 shows the fabricated prototype of a 4-element MIMO antenna array designed. The overall compact square layout optimizes space utilization and ensures structural symmetry, which contributes to stable far-field radiation characteristics. This fabricated prototype is intended for sub-GHz (0.9 GHz) and 2.4–2.6 GHz ISM/LTE bands, as validated in the simulated and measured results, making it suitable for modern wireless communication applications such as IoT, Wi-Fi, Bluetooth, and LTE systems.

Figure 16 indicates the simulated and measured reflection coefficients with a good agreement between them. It shows significant dips around 1 GHz and 2.5 GHz with return losses well below −10 dB. The device is well matched and likely intended to operate effectively at these resonant frequencies.

The transmission coefficients shown in Figure 17 reveal frequency-selective behavior, with transmission dips occurring at specific targeted bands. The simulated and measured overall responses matched well, while minor discrepancies are found due to the variation in fabrication process. The reflection and transmission characteristics collectively confirm that the antenna achieves multiple frequency bands.

The polar plots (Figure 18) illustrate the simulated and measured radiation patterns at frequencies of 0.9 GHz and 2.5 GHz. The radiation pattern is nearly omnidirectional at 0.9 GHz, with the maximum simulated gain of 2.9 dBi at 60° and measured gain of 2 dBi at 13°. The patterns become more directional at higher frequency, with slight deviations between measured and simulated results. The simulated gain at 2.5 GHz is 1.9 dBi at 85° and measured gain 1.7 dBi at 2°. Overall, the radiation performance remains stable across frequencies, indicating steady

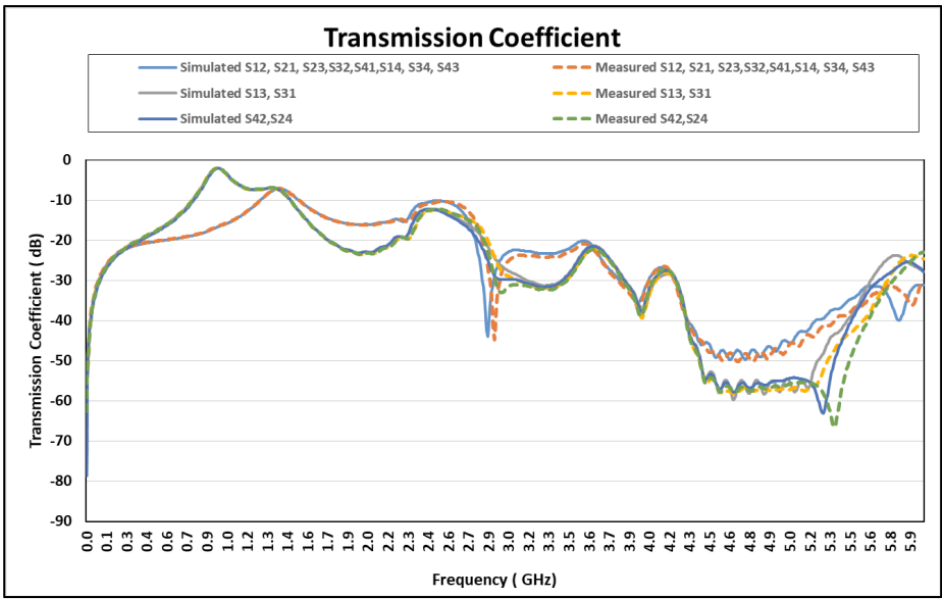

FIGURE 17. Simulated vs measured transmission coefficient of MIMO antenna.

TABLE 2. A comparison of the referred and proposed antennas.

S. N.	Referred Paper	No. of Elements	Peak gain (dBi)	ECC	Diversity gain (dB)	Optimization/ coupling-reduction used	Size (mm)	Bands covered
1	Proposed antenna	4	3.64	< 0.005	10	Slot, Slit, DGS and twin hexagonal concentric ring	$60 \times 60 \times 1.6$	0.91 & 2.5 GHz
2	[6]	2	NR	< 0.002	9.999	Two-monopole arrays + T-stub loading	32×32 (board)	2.89–12 GHz (UWB)
3	[7]	4	> 6	< 0.02	NR	Dual-polarized patches + I-shaped DGS	$\approx 50 \times 40 \times 1.6$	5.5 GHz ($\approx 2.2\%$ BW)
4	[9]	2	6.1	< 0.05	10	Common-ground CPW + fractal radiators (single-sided)	$60 \times 30 \times 1.6$	3.1–10.6 GHz (UWB)
5	[16]	2	6	< 0.05	~ 10	DGS (etched ground) for coupling reduction	$0.92\lambda \times 0.73\lambda \times 0.03\lambda$ at 5.5 GHz	Sub-6 GHz (broadband, UWB context)
6	[21]	2	10.8	≈ 0.001	≈ 9.99	Novel decoupling structure; EBG-style idea	$25 \times 10 \times 1.52$	25.25–29.85 GHz (mmWave)
8	[26]	4	NR	< 0.05	9.99	Compact isolation structure; UWB layout	$33 \times 33 \times 0.203$	25–50 GHz (UWB, mmWave)

directional behavior and good agreement between simulated and measured results.

5. COMPARATIVE ANALYSIS WITH EXISTING WORK

The proposed four-element MIMO antenna provides competitive performance compared with existing available designs. As Compared to previously reported MIMO antenna designs, the proposed four-element antenna achieves dual-band operation at 0.9 GHz and 2.4–2.6 GHz within a compact size, offering superior versatility for IoT and wireless applications. In contrast to traditional designs, this study uses triangular slots, twin grooves, and an optimized ground plane to improve isolation and impedance bandwidth. Overall, it balances compactness, dual-band coverage, and high isolation for sub-6 GHz applications. In Table 2, the suggested antenna is compared with the most current MIMO antennas.

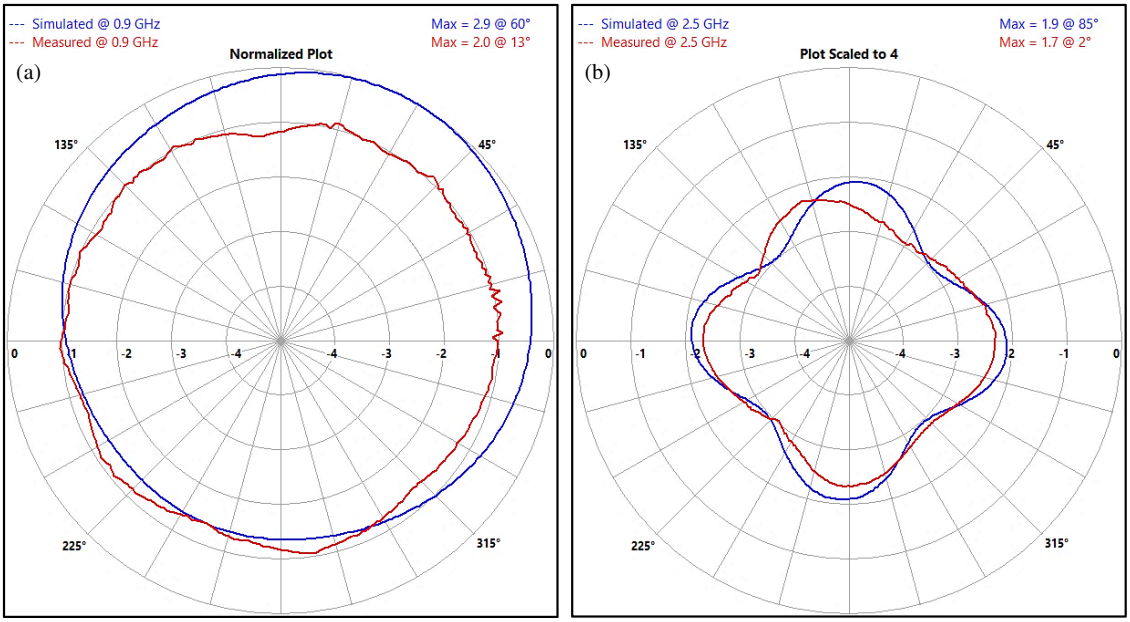

FIGURE 18. Simulated vs measured E plane radiation pattern of MIMO antenna. (a) 0.9 GHz, (b) 2.5 GHz.

6. CONCLUSION

In this research, a compact four-element MIMO antenna is designed and validated experimentally. The antenna employs a rectangular microstrip patch integrated with twin grooves, triangular slots, and a modified ground plane to achieve multi-resonant characteristics, and better isolation performance. The overall geometry is optimized within a compact footprint of $60 \times 60\,\text{mm}^2$, and it is suitable for portable systems where size efficiency is crucial. The proposed antenna reveals effective dual-band response around 0.9 GHz and 2.4–2.6 GHz. The lower band at the 0.9 GHz band, a return loss of -16.16 dB with a gain of 2.9 dBi is achieved, which is suitable for long-range, low-power connectivity useful for GSM and LoRa applications. On the other hand at higher frequencies, better performance is observed, with return losses of -31.19 dB, isolation levels below -15 dB, and stable radiation gains ranging 3.1–3.6 dBi suitable for ISM/LTE bands (Band 8, Band 7, Band 41, and Band 53). The fabricated prototype offers close agreement with simulated results, thereby validating the proposed design. Overall, the proposed antenna offers a compact, cost-effective, and high-performance solution suitable for IoT (2.4 GHz) networks, smart home technologies, industrial automation systems, and portable wireless devices.

REFERENCES

[1] Ali, E. M., M. Alibakhshikenari, N. A. Elmunim, B. S. Virdee, N. Rashid, D. Mariyanayagam, M. A. Chaudhary, N. A. Abbasi, P. Livreri, and T. Saber, "Defected ground structure antenna array with metasurface inspired interlinked CSRR for 5G millimeter wave applications," *Scientific Reports*, Vol. 15, No. 1, 28534, 2025.

[2] Khade, S. S., D. B. Bhoyar, K. Kotpalliwar, C. V. Bawankar, and M. S. Kimmatkar, "Four element EC slot MIMO antenna for WLAN, Wi-Fi and 5G applications," *Progress In Electromagnetics Research C*, Vol. 139, 147–158, 2024.

[3] Elabd, R. H., A. J. Al-Gburi, and A. A. Megahed, "Compact circular MIMO antenna with defected ground structure (DGS) for improved isolation in 5G sub-6 GHz mobile systems," *Results in Engineering*, Vol. 27, 105737, 2025.

[4] Dhananjeyan, R., S. Ramesh, D. R. Kumar, and O. P. Kumar, "Compact octagonal MIMO antenna system for broadband applications with enhanced isolation and wideband performance," *Scientific Reports*, Vol. 15, No. 1, 18921, 2025.

[5] Xia, K., Y.-Q. Bao, and H.-F. Zhang, "Defected ground structure-based circularly polarized MIMO filtering dielectric resonator antenna," *Physics Letters A*, Vol. 549, 130589, 2025.

[6] Tirado-Mendez, J. A., H. Jardon-Aguilar, R. Linares-Miranda, E. Fritz-Andrade, R. Flores-Leal, A. Perez-Miguel, and R. Gomez-Villanueva, "Compact size 4-port MIMO antenna formed with two-branches strip-monopoles with bandwidth enhancement using a T-stub line-load," *Applied Sciences*, Vol. 15, No. 7, 3757, 2025.

[7] Tran-Huy, D., C. Do-Manh, H. Pham-Duy, N. Tran-Viet-Duc, H. Tran, D. Nguyen-Tien, and N. Hussain, "Compact four-port MIMO antenna using dual-polarized patch and defected ground structure for IoT devices," *Sensors*, Vol. 25, No. 14, 4254, 2025.

[8] Barua, H. R. and I. A. Chowdhury, "Design and analysis of mm-Wave MIMO antenna with DGS for 5G applications," *Journal of Electrical Systems and Information Technology*, Vol. 12, Article number 17, Jun. 2025.

[9] Shailesh, G. S., S. Kumar, D. Sharma, B. Goyal, and N. F. Soliman, "A common grounded ultra-wideband diversity/MIMO antenna with high inter-element isolation," *Scientific Reports*, Vol. 15, 27334, 2025.

[10] Rani, P., M. K. Gaur, P. Tiwari, M. Kaushik, A. Shastri, and V. Gahlaut, "Design and implementation of a compact ultra-wideband reconfigurable antenna using RF MEMS switch technology," *Discover Electronics*, Vol. 2, Article number 32, 2025.

[11] Patel, A., T. Upadhyaya, P. R. Girjashankar, M. V. Swati, and O. P. Kumar, "Enhanced isolation in aperture fed dielectric resonator MIMO antennas for 5G sub 6 GHz applications," *Scientific Reports*, Vol. 15, No. 1, 10653, 2025.

[12] Elabd, R. H. and A. J. A. Al-Gburi, "Ultra-compact 4-port MIMO antenna with defected ground structure and SAR analysis for 28/38 GHz 5G mobile devices," *Journal of Electromagnetic Waves and Applications*, Vol. 38, No. 9, 1000–1025, 2024.

[13] Saleh, S., T. Saeidi, N. Timmons, B. Alali, F. Razzaz, and A. A. Althuway, "Compact ultra-wide band two element Vivaldi non-uniform slot MIMO antenna for body-centric applications," *Results in Engineering*, Vol. 24, 102839, 2024.

[14] Jhunjhunwala, V. K., P. Kumar, A. P. Parameswaran, P. R. Mane, O. P. Kumar, T. Ali, S. Pathan, S. Vincent, and P. Kumar, "A four port flexible UWB MIMO antenna with enhanced isolation for wearable applications," *Results in Engineering*, Vol. 24, 103147, 2024.

[15] Banerjee, J., A. Gorai, and R. Ghatak, "A compact UWB MIMO antenna augmented with isolation improvement structures in situ with ground stubs and slots," *International Journal of Microwave and Wireless Technologies*, Vol. 16, No. 3, 454–465, 2024.

[16] Elalaouy, O., M. El Ghzaoui, and J. Foshi, "Mutual coupling reduction of a two-port MIMO antenna using defected ground structure," *e-Prime — Advances in Electrical Engineering, Electronics and Energy*, Vol. 8, 100557, 2024.

[17] Elabd, R. H. and A. A. Megahed, "Isolation enhancement of a two-orthogonal printed elliptical slot MIMO antenna array with EBG structure for millimeter wave 5G applications," *Discover Applied Sciences*, Vol. 6, Article number 222, 2024.

[18] Gaid, A. G. S. A., A. N. S. Ali, and M. A. Alomari, "A compact microstrip antenna with dual thin slits for high-capacity data streaming in the 38 and 39 GHz bands for 5G applications," *Results in Engineering*, Vol. 24, 103411, 2024.

[19] Güler, C. and S. E. B. Keskin, "A novel high isolation 4-port compact MIMO antenna with DGS for 5G applications," *Micromachines*, Vol. 14, No. 7, 1309, 2023.

[20] Dala Pegorara Souto, V., P. S. Dester, M. S. P. Facina, D. G. Silva, F. A. P. de Figueiredo, *et al.*, "Emerging MIMO technologies for 6G networks," *Sensors*, Vol. 23, No. 4, 1921, 2023.

[21] Islam, T., F. Alsaleem, F. N. Alsunaydih, and K. Alhassoon, "Mutual coupling reduction in compact MIMO antenna operating on 28 GHz by using novel decoupling structure," *Micromachines*, Vol. 14, No. 11, 2065, 2023.

[22] Chen, S., N. Lu, J. Sun, C. Zhou, C. Li, and D. Wu, "High-isolation wideband MIMO antenna with offset T-shaped slots for 5G/WLAN applications," *Frontiers in Physics*, Vol. 10, 986558, 2022.

[23] Ahmed, B. T. and I. F. Rodríguez, "Compact high isolation UWB MIMO antennas," *Wireless Networks*, Vol. 28, No. 5, 1977–1999, 2022.

[24] Xing, H., X. Wang, Z. Gao, X. An, H.-X. Zheng, M. Wang, and E. Li, "Efficient isolation of an MIMO antenna using defected ground structure," *Electronics*, Vol. 9, No. 8, 1265, 2020.

[25] Ghasemi, M., "MIMO antenna optimization for millimeter-wave 5G applications using machine learning," *Discover Electronics*, Vol. 2, 58, 2025.

[26] Alibakhshikenari, M., E. M. Ali, I. U. Din, B. S. Virdee, S. Ullah, S. Khan, C. H. See, T. Saber, and E. Limiti, "Millimeter-wave MIMO array with low interactions between its antenna elements for fifth generation wireless communication networks," *Journal of Infrared, Millimeter, and Terahertz Waves*, Vol. 46, No. 7, 46, Jun. 2025.

[27] Alwatban, F., N. Almushaiti, K. Almoshaiti, A. Alnogithan, A. Alsalman, A. Alhumaid, and M. Shaban, "Design and implementation of reconfigurable MIMO antennas for radar applications," *Journal of Electrical Engineering*, Vol. 76, No. 3, 284–299, Jun. 2025.

[28] Irshad, A., A. Kosasih, V. Petrov, and E. Björnson, "Pre-optimized irregular arrays versus moveable antennas in multi-user MIMO systems," *arXiv preprint arXiv:2502.03994*, Feb. 2025.

[29] Min, H., X. Li, R. Li, and Y. Zeng, "Integrated localization and communication with sparse MIMO: Will virtual array technology also benefit wireless communication?" *arXiv preprint arXiv:2502.18241*, Feb. 2025.

[30] Tiwari, R. N., D. Sharma, P. Singh, and P. Kumar, "Design of dual-band 4-port flexible MIMO antenna for mm-Wave technologies and wearable electronics," *IEEE Access*, Vol. 12, 96 649–96 659, Jun. 2024.